Journal of Materials Chemistry C

ROYAL SOCIETY OF CHEMISTRY

PAPER

View Article Online
View Journal | View Issue

Cite this: J. Mater. Chem. C, 2024, 12, 11907

A long-term stable zero-thermal-quenching blue-emitting phosphor for sustainable and human-centric lighting†

Heng Dai,[ab] Xinran Wang,[a] Zhichao Liu,[a] Jian Zhang,[a] Xuhui Xu *[a] and Ge Zhu *[b]

Received 19th May 2024,
Accepted 26th June 2024

DOI: 10.1039/d4tc02056a

rsc.li/materials-c

Human-centric lighting can reduce the proportion of harmful short-wave blue light, relieve visual fatigue, and regulate the normal physiological rhythm of human beings. However, the development of healthy lighting is stringently restricted because few blue phosphors can be efficiently pumped by violet LED chips (395–405 nm). Herein, we have developed a blue-emitting phosphor $Sr_{1.91}Mg_{0.66}Al_{22.33}O_{36}:Eu^{2+}$ with high internal quantum efficiency under 395 nm excitation, which contains more cyan and fewer blue components. Surprisingly, the material shows zero-thermal-quenching even when the temperature is as high as 200 °C. The defect related thermal quenching mechanism was demonstrated through thermoluminescence and electron paramagnetic resonance analysis. Moreover, the phosphor exhibits good long-term stability when it is exposed to air for 2.5 years. Finally, a blue light weakened warm white light-emitting diode (WLED) has been achieved by packaging commercial phosphors and $Sr_{1.91}Mg_{0.66}Al_{22.33}O_{36}:Eu^{2+}$ on a 395 nm LED chip, with a low correlated color temperature of 3919 K and a high color index of 90.2. All results indicate that the $Sr_{1.91}Mg_{0.66}Al_{22.33}O_{36}:Eu^{2+}$ phosphor has the ability to promote sustainable and human-centric lighting.

1. Introduction

The daily routine and lifestyle habits of human beings are closely related to the spectral components of sunlight.[1–3] For example, bright white light during the morning and midday makes it easier to get excited and stay in good working condition, due to the higher blue light component in white light that suppresses the secretion of melatonin. Conversely, white light in the afternoon or evening has a lower blue content, which is more likely to make people sleepy due to increased melatonin secretion.[4–7] However, the most mature solid-state lighting solution today still combines a blue light-emitting GaN chip with a yellow light-emitting phosphor ($YAG:Ce^{3+}$) to obtain white light.[8–10] Unfortunately, the cold white light produced by this combination inevitably contains a high blue component, and prolonged exposure to a strong blue light environment not only causes sleep disorders, but also induces irreversible eye diseases, which seriously affect human life and health.[11–15] Therefore, it is necessary and urgent to develop human-centric sustainable and healthy lighting technology.

The current study shows that, as a new alternative strategy, combining long-wavelength ultraviolet (LWUV) LED chips with red, green, and blue phosphors not only achieves full spectrum emission but also greatly reduces the intensity of blue light.[16–18] Nevertheless, limited by semiconductor chip technology, the efficiency of UV-LED chips decreases with the decrease of excitation wavelength and there are few reports on high efficiency blue phosphors that can be excited by LWUV-LED chips.[19] Therefore, it is urgent to develop trichromatic (red/green/blue) phosphors that can maintain high efficiency and long-term stability under LWUV light excitation. Unfortunately, until now the inherent Stokes loss has resulted in few blue phosphors having high internal quantum efficiency (IQE) under LWUV excitation compared with red and green phosphors.[20,21] Although the currently reported blue phosphors, such as $Sr_3MgSi_2O_8:Eu^{2+}$ and $Ca_5(PO_4)_3Cl:Eu^{2+}$, have a wide absorption range in the ultraviolet region, their thermal stability and efficiency cannot well meet the requirements of practical applications.[22,23] Although the commercial blue phosphor $BaMgAl_{10}O_{17}:Eu^{2+}$ ($BAM:Eu^{2+}$) has high IQE, its thermal quenching behavior leads to a decrease in the luminescence efficiency of the device in practical applications.[24,25] In

[a] Yunnan Joint International Laboratory of Optoelectronic Materials and Devices, Faculty of Materials Science and Engineering, Kunming University of Science and Technology, Kunming Yunnan 650093, Yunnan, China. E-mail: xuxuh07@126.com
[b] Key Laboratory of New Energy and Rare Earth Resource Utilization of State Ethnic Affairs Commission, Key Laboratory of Photosensitive Materials & Devices of Liaoning Province, College of Physics and Materials Engineering, Dalian Minzu University, 18 Liaohe West Road, Dalian 116600, P. R. China. E-mail: zhuge@dlnu.edu.cn

† Electronic supplementary information (ESI) available. See DOI: https://doi.org/10.1039/d4tc02056a

addition, when exposed to air for a long time, the valence state of rare earth ions is easily changed from Eu^{2+} to Eu^{3+}, resulting in a further decrease in the luminescence efficiency of the device.[26,27] Therefore, the development of blue phosphors with high IQE, zero-thermal-quenching and long-term stability under LWUV (395–405 nm) excitation is the key to achieving sustainable and human-centric lighting.

In this work, we report a zero-thermal-quenching blue-emitting $Sr_{1.91}Mg_{0.66}Al_{22.33}O_{36}:Eu^{2+}$ (SMAO:Eu^{2+}) phosphor that can be excited at 395 nm and exhibits high IQE and long-term stability. The SMAO:Eu^{2+} phosphor exhibits zero-thermal-quenching behavior at 200 °C and contains fewer blue light and more cyan light components compared to the commercially available BAM:Eu^{2+} phosphor. More satisfactorily, the phosphor still sustains a stable phase structure and high IQE when exposed to air for more than 2.5 years. Finally, a prototype device driven by a 395 nm LED employing SMAO:Eu^{2+} generates a warm white light. It can effectively reduce the intensity of blue light and compensate the defects of cyan light without significantly suppressing the melatonin production. The high efficiency SMAO:Eu^{2+} blue phosphor reported in this paper not only reveals an excellent zero-thermal-quenching phenomenon, but also demonstrates broad prospects in sustainable and human-centric lighting.

2. Results and discussion

2.1 Crystal structure and morphology analysis

The X-ray diffraction (XRD) patterns of the SMAO:xEu^{2+} ($0 \leq x \leq 0.02$) phosphors are presented in Fig. 1a. All XRD patterns are consistent with the Inorganic Crystal Structure Database (ICSD#82105) with the increasing concentration of Eu^{2+}, indicating that the Eu^{2+} ion successfully enters the host. Besides, the Rietveld refinement of SMAO:0.015Eu^{2+} was carried out through the General Structural Analysis System (GSAS) program, as shown in Fig. 1b and Fig. S1 (ESI†). The crystallographic parameters of the refined SMAO:0.015Eu^{2+} sample are listed in Table S1 (ESI†). SMAO:0.015Eu^{2+} samples belong to the space group $P\bar{6}m2$, $a = b = 5.583$ Å, $c = 22.116$ Å and $V = 598.832$ Å^3. The phase purity of the prepared sample is confirmed by the convergence factor $R_p = 9.94\%$, $R_{wp} = 13.86\%$ and $\chi^2 = 1.68$, and the associated atomic positions and thermal vibration parameters are listed in Table S2 (ESI†). The spatial structure of a unit cell of SMAO is shown in Fig. S2 (ESI†). Sr^{2+} ions have two different coordination environments, $Sr1O_{12}$ and $Sr2O_9$. In the SMAO host, Eu^{2+} ions are most likely to occupy the Sr^{2+} ion position due to the same valence state and approximate ionic radius ($R_{Sr^{2+}} = 1.44$ Å for CN = 12, $R_{Sr^{2+}} = 1.31$ Å for CN = 9, $R_{Eu^{2+}} = 1.30$ Å for CN = 9, and $R_{Mg^{2+}} = 0.72$ Å for CN = 6, where R stands for the ionic radius and CN is the coordination number).[28]

To further confirm the phase component, the morphology of the prepared SMAO:0.015Eu^{2+} phosphor is studied *via* field emission scanning electron microscopy (FE-SEM), as shown in Fig. 2a. Interestingly, the morphology of the samples prepared by a high temperature solid-state method no longer shows irregular particles but regular hexagonal sheets with a side length of about 3 μm, indicating high phase purity and good crystallization properties. Fig. 2b shows the energy dispersive X-ray spectra (EDS) mapping images. It is found that the sample contains evenly distributed Sr, Mg, Al, O and Eu elements, further confirming the successful doping of Eu^{2+} into the SMAO host. Moreover, the atomic percentage analysis of the SMAO:0.015Eu^{2+} sample is quite close to the theoretical ratio, as shown in Fig. 2c. Fig. S3(a and b) (ESI†) show the high-resolution transmission electron microscopy (HR-TEM) pattern and the TEM image of the sample, respectively. The plane spacing is measured to be 0.319 nm, corresponding to the (012) crystal plane of SMAO. Fig. S3c (ESI†) is a fast Fourier transform (FFT) image of the selected region, which shows that the (012) and (025) crystalline planes of a hexagonal SMAO crystal. These results further verify the successful synthesis and high crystallinity of SMAO:Eu^{2+} and are consistent with previous XRD results.

2.2 Photoluminescence properties and Eu^{2+} site preference analysis

As we all know, the light absorption capacity of phosphors plays an important role in luminescence materials. Here, we measured the diffuse reflectance spectra (DRS) of the samples and the corresponding results are shown in Fig. 3a. Significantly, all samples exhibit a broad absorption band in the range of 230–430 nm and

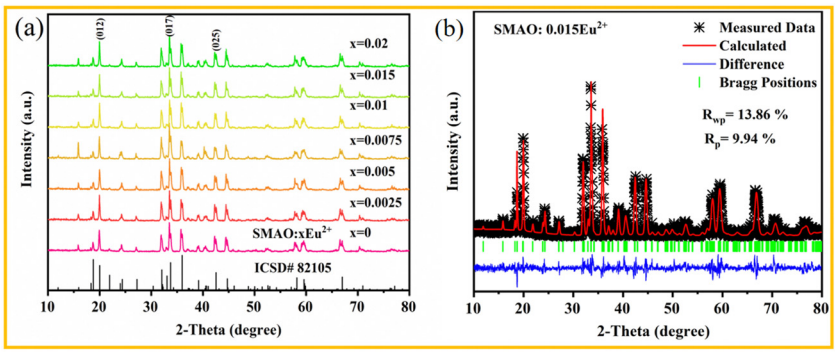

Fig. 1 (a) XRD patterns of the SMAO:xEu^{2+} ($0 \leq x \leq 0.02$) samples and (b) Rietveld structure refinement patterns of SMAO:0.015Eu^{2+}.

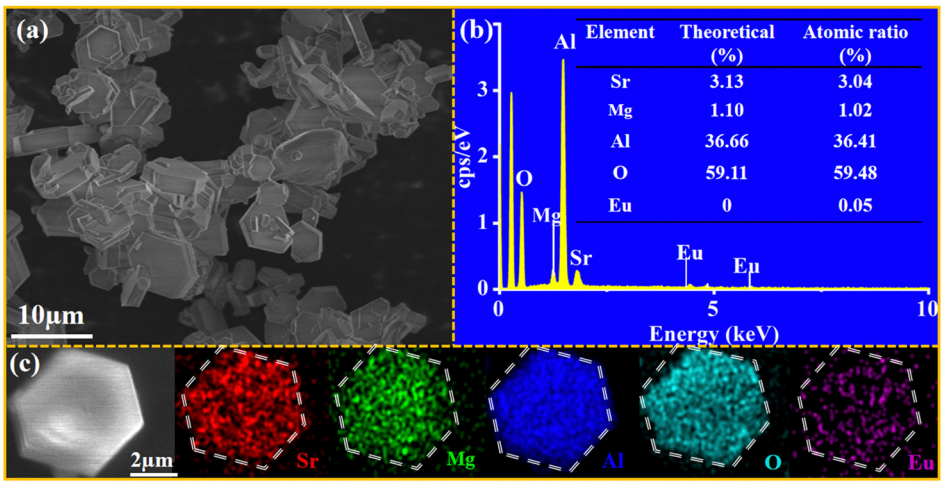

Fig. 2 (a) The SEM images of the SMAO:0.015Eu^{2+} phosphor; (b) EDS mapping images of elements; and (c) the content of the corresponding elements.

can be attributed to the 4f → 5d transition of the Eu^{2+} ion. Fig. 3b shows the photoluminescence excitation (PLE) and photoluminescence (PL) spectra of the SMAO:$x$$Eu^{2+}$ ($0.0025 \leq x \leq 0.02$) samples. The maximum peak position of the PLE spectra is at 332 nm, and the spectral range is consistent with the above DRS. The maximum emission peak position of SMAO:$x$$Eu^{2+}$ ($0.0025 \leq x \leq 0.02$) is around 458 nm, attributed to Eu^{2+} ion transition from 5d → 4f. The emission intensity of the SMAO:$x$$Eu^{2+}$ ($0.0025 \leq x \leq 0.02$) samples increases with increasing x, and the optimal doping concentration is determined to be 0.015 (Fig. S4a, ESI†). The interaction types between Eu^{2+} can be obtained using eqn (S1) and (S2) (ESI†). Fig. S4b (ESI†) gives the linear relationship between log (I/x) and log (x). Accordingly, the value of θ is 3.172, which is closest to 6, indicating that the d–d interaction plays a dominant role in the energy transfer process.[22] Fig. 3c presents the decay curves of SMAO:$x$$Eu^{2+}$ ($0.0025 \leq x \leq 0.02$) phosphors, which can fitted by the double exponential eqn (S3) (ESI†). The average decay times of SMAO:$x$$Eu^{2+}$ ($0.0025 \leq x \leq 0.02$) samples are calculated to be 1.217, 1.213, 1.209, 1.205, 1.194 and 1.179 μs for x = 0.0025, 0.005, 0.0075, 0.01, 0.015 and 0.02, respectively, gradually decreasing the lifetime from 1.217 to

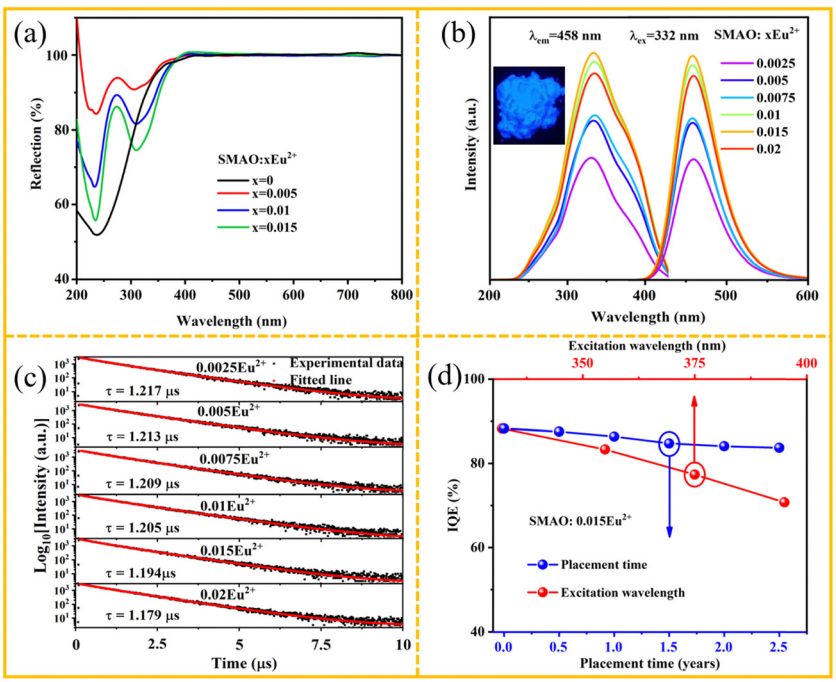

Fig. 3 (a) The DRS of the SMAO:$x$$Eu^{2+}$ (x = 0, 0.005, 0.01 and 0.015) phosphors; (b) the PLE and PL spectra (inset: photograph of the SMAO:Eu^{2+} phosphor) and (c) decay curve of the SMAO:$x$$Eu^{2+}$ ($0.0025 \leq x \leq 0.02$) phosphors; and (d) the IQE of the SMAO:0.015Eu^{2+} phosphor at different excitation wavelengths and when placed in air for various years.

1.179 μs with increasing Eu^{2+} concentration. The slight change in the lifetime indicates weak non-radiative energy transfer between Eu^{2+} ions, which is beneficial for obtaining highly efficient phosphors.[25]

So far, few works have focused on the long-term stability of phosphors. However, long-term stability is crucial for the practical application of LED devices. In this study, the environmental stability of SMAO:0.015Eu^{2+} was investigated by placing the phosphor in air for 2.5 years and analyzing the XRD, PL and IQE. Incredibly, it exhibits just 5% loss of IQE after being placed in air for 2.5 years (the blue line in Fig. 3d). The XRD analysis of SMAO:0.015Eu^{2+} indicates that SMAO:0.015Eu^{2+} retains a stable phase structure (Fig. S5a, ESI†). The PL spectra reveal virtually no change in the peak shape and position upon 332 nm excitation (Fig. S5b, ESI†). The commercial BAM:Eu^{2+} after industrial post-processing and material optimization shows incredible oxidation resistance (≈15 years).[26] Similar techniques could be applied to SMAO:0.015Eu^{2+} to improve chemical stability further. Although a preliminary analysis of the optical properties of this material is beneficial, SMAO:0.015Eu^{2+} must effectively convert an UV-LED chip (λ_{ex} ≈ 395 nm) into blue light to be suitable for human-centric lighting.[29] The IQE of SMAO:0.015Eu^{2+} under different violet excitations provided in Fig. 3d (red line) and Fig. S6(a–d) (ESI†), respectively. The IQE of SMAO:0.015Eu^{2+} gradually decreases with the increase of the excitation wavelength from 332 nm to 395 nm, but the IQE remains at 70.76% under the excitation at 395 nm. Table 1 compares the IQE of SMAO:0.015Eu^{2+} and other blue luminescent materials excited at 395 nm. We found that our samples have a higher quantum efficiency than most blue luminescent materials. The excellent IQE values and long-term stability demonstrate that the designed blue-emitting phosphor has powerful potential for application in sustainable and human-centric lighting.

Fig. 4a shows the PL spectrum of the sample at 80 K. In fact, the asymmetric blue emission bands of the SMAO:0.015Eu^{2+} phosphor can be fitted with two Gaussian components, and it suggests that there may be two different Eu^{2+} luminescent centers in the SMAO lattice. The maximum value is located at 450 nm (Eu1) and 480 nm (Eu2), respectively. Moreover, the luminous energy of Eu^{2+} ions is related to their coordination environment, which can estimate by the eqn (S4) (ESI†).[38] In this case, the emitted energy is directly proportional to the values of n and r. In other words, if the values of n and r are larger, the emission energy is larger. The coordination numbers (n) of the Sr1 and Sr2 sites are 12 and 9, and the ionic radius (r) is 1.44 Å and 1.31 Å, respectively. It is clear that the emission peak of high energy is attributed to the Eu^{2+} occupied Sr1 (Eu1) site, while the emission peak of low energy is attributed to Eu^{2+} in the Sr2 (Eu2) site. Fig. 4b shows the temperature-dependent normalized PL spectra of SMAO:0.015Eu^{2+} phosphor in the range from 80 to 290 K. The normalized PL spectra are gradually blue-shifted with increasing temperature, which is caused by lattice thermal expansion resulting in a smaller crystal field splitting on the one hand and a phonon-assisted excitation from a lower-energy to a higher-energy sub-level of the excited states of Eu^{2+} on the other.[39,40]

The normalized PLE and PL spectra of SMAO:0.015Eu^{2+} under different excitations and emissions are shown in Fig. 4c. The difference between PLE and PL further suggests that Eu^{2+} should have two different luminescence centers. To further prove this conjecture, the decay curves of the emissions at 420 nm and 560 nm under 332 nm excitation are recorded, respectively, as shown in Fig. 4d. The decay curves can be well fitted by the double exponential model, and the lifetime values are determined to be 0.93 μs (420 nm) and 1.21 μs (560 nm), respectively. Therefore, the differences of the lifetimes further verify the two emission centers.[36] Fig. S7 (ESI†) clearly shows that the emission spectrum of the SMAO:Eu^{2+} phosphor has more cyan and fewer blue components, and a wider full width at half maximum compared with the BAM:Eu^{2+} phosphor, which confirms its advantages as a sustainable and human-centric full-spectrum WLED.

Table 1 Comparison of the luminescence properties of SMAO:0.015Eu^{2+} and some blue and commercial phosphors

Phosphors	λ_{ex} (nm)	λ_{em} (nm)	IQE (%)	EQE (%)	Ref.
$K_2SiF_6:Mn^{4+}$	468	635	96.92	30.84	8
$Y_3Al_5O_{12}:Ce^{3+}$	460	530	89	46	11
$K_3AlP_3O_9N:Eu^{2+}$	395	454	58.3	24.5	15
$Sr_3MgSi_2O_8:Eu^{2+}$	395	460	23.12	—	22
$Ca_5(PO_4)_3Cl:Eu^{2+}$	395	456	25	11	23
$BaMgAl_{10}O_{17}:Eu^{2+}$	395	450	90	68.2	25
$Na_2MgPO_4F:Eu^{2+}$	395	456	60	35	26
$Ca_9NaSc_{0.667}(PO_4)_7:Eu^{2+}$	395	480	14	—	30
$Na_3Ba_2Ca(PO_4)_3:Eu^{2+}$	395	445	27	—	31
$Ca_8ZnGa_{0.4}La_{0.6}(PO_4)_7:Eu^{2+}$	395	470	14.31	—	32
$CaYGaO_4:Bi^{3+}$	395	435	37	—	33
$Sr_3Lu_2Ge_3O_{12}:Bi^{3+}$	395	466	49.6	27	34
$SrSi_6N_8:Eu^{2+}$	395	450	38	—	35
$Na_3Sc_2(PO_4)_3:Eu^{2+}$	395	458	21	—	36
$BaHfSi_3O_9:Eu^{2+}$	395	470	47.5	18	37
SMAO:0.015Eu^{2+}	**395**	**458**	**70.76**	**19.76**	This work

2.3 Zero-thermal-quenching behavior and defect-related thermal quenching mechanism analysis

As one of the critical factors for evaluating the properties of phosphors, the thermal quenching behavior of the SMAO:0.015Eu^{2+} sample was measured as shown in Fig. 5a. As the temperature increases, the integral emission intensity exhibits an anomalous anti-thermal-quenching characteristic, that is, the emission intensity does not decrease but increase with the rise of temperature.[41,42] Surprisingly, when the temperature rises to 150 °C, the integral emission intensity is enhanced to 112% of its initial intensity at room temperature and even remains at 102% at 200 °C. However, for commercial BAM:Eu^{2+}, the integral emission intensity drops to 86% and 77% at 150 °C and 200 °C, respectively.[43] Moreover, a slight blue-shift of the emission peaks can be observed with the increase of temperature, which is for the same reason as that given in Fig. 4b. In addition, the non-radiative process of charge carriers coupled to phonons caused by rise of temperature leads to the FWHM of the emission peak from 2716 (0.113 eV) to 3068 cm^{-1} (0.150 eV)

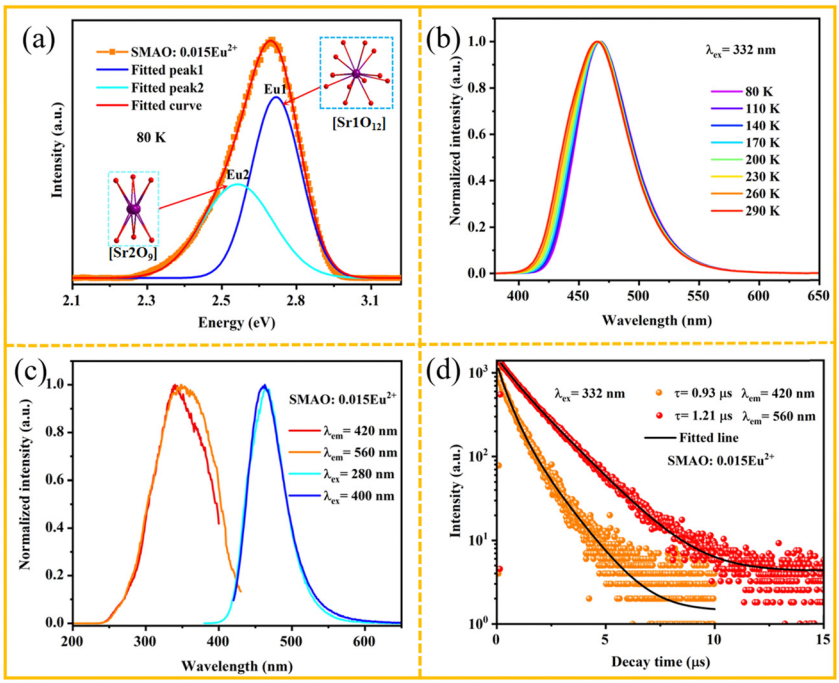

Fig. 4 (a) Gaussian fitting spectrum of SMAO:0.015Eu^{2+} at 80 K; (b) normalized PL spectra of SMAO:0.015Eu^{2+} from 80 K to 290 K; (c) normalized PLE and PL spectra for SMAO:0.015Eu^{2+} under different excitations and emissions; and (d) decay curve of the SMAO:0.015Eu^{2+} sample monitored under 420 and 560 nm excitation at 332 nm.

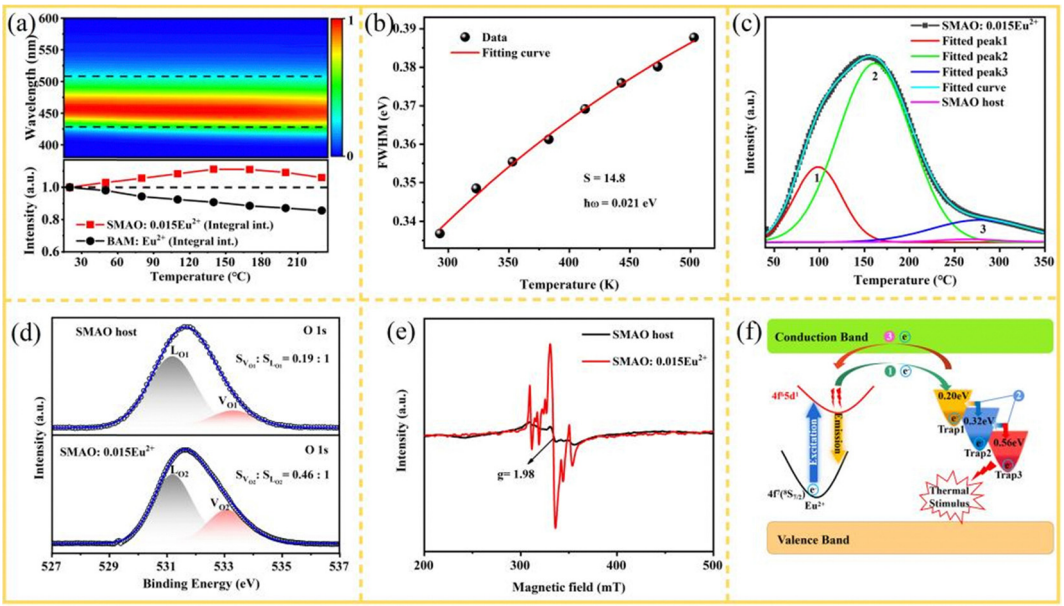

Fig. 5 (a) Two-dimensional diagram of TQ behaviors of SMAO:0.015Eu^{2+} and integral emission intensity of SMAO:0.015Eu^{2+} *versus* commercial BAM:Eu^{2+} phosphors at different temperatures; (b) fitted Huang–Rhys factor (S) and the phonon energy ($\hbar\omega$); (c) the TL fitted curves of SMAO:0.015Eu^{2+} and SMAO samples; (d) the XPS spectra and (e) EPR spectra of the SMAO host and SMAO:0.015Eu^{2+}; and (f) the schematic illustration of the abnormal TQ behavior.

as shown in Fig. 5b, which can be well fitted using the formula S(5) (ESI†). Here, the calculations results are S (Huang–Rhys parameter) = 14.8, $\hbar\omega$ (phonon energy) = 0.021 eV. Strong electron–phonon coupling occurs when $S > 5$,[27] indicating the strong electron–phonon coupling (EPC) effect in SMAO:Eu^{2+} phosphors. Notably, the expected zero-thermal-quenching luminescence properties of the material seem inconsistent with the strong EPC effect, as shown in Fig. 5a. Lots of works have

reported that the zero-thermal-quenching behavior at high temperatures can be assigned to the thermally activated luminescence of the electrons trapped by the defect levels.[44] However, most of the research work lacks sufficient evidence to prove the characteristics of defects.[45–49] In this work, the defect types in the sample are analyzed in detail by measuring thermoluminescence (TL), X-ray photoelectron spectra (XPS) and electron paramagnetic resonance (EPR). The TL technology is employed to ensure the existence and distribution of defects, as shown in Fig. 5c. The TL curve of the SMAO host is almost a horizontal line compared with that of Eu^{2+} doped samples, indicating that continuous defects are introduced after doping Eu^{2+}. Then the TL curve of the SMAO:0.015Eu^{2+} sample is well fitted to three peaks centered at around 97 °C (trap 1), 167 °C (trap 2) and 282 °C (trap 3), respectively, and the corresponding trap depth can be evaluated to be 0.74, 0.88 and 1.11 eV based on the following equation E_T (trap depths) = T (kelvin)/500 eV.[50] Considering that SMAO:0.015Eu^{2+} and SMAO are synthesized in a reducing atmosphere, the defect centers may be related to intrinsic oxygen vacancies.[51] To further elucidate the defect characteristics, XPS analysis of SMAO:0.015Eu^{2+} is carried out as shown in Fig. S7a (ESI†).

The doped Eu detected in the XPS survey spectrum indicates that the Eu^{2+} ion is successfully introduced into the lattice. The XPS of the Eu 3d orbitals for the SMAO:0.015Eu^{2+} phosphor is shown in Fig. S7b (ESI†).[52] The atomic percentages of experimental and theoretical values for each element are shown in Table S3 (ESI†). The results show that the composition of the O element is higher than the theoretical value, while the other element can correspond well. Moreover, the XPS peaks of the O 1s orbital of the SMAO host and SMAO:0.015Eu^{2+} can be Gaussian fitted to two peaks at 531.2 eV and 533.1 eV as shown in Fig. 5d. Accordingly, the relatively low binding energy peak is mainly associated with the lattice oxygen (L_O), while the peak located at 533.1 eV is associated with the oxygen vacancies (V_O).[53] After doping with Eu^{2+} ions, the area ratio of V_O to L_O in the SMAO:0.015Eu^{2+} sample significantly increased compared to the SMAO host sample, indicating that the V_O concentration is significantly increased after doping Eu^{2+}, which coincides with the change of V_O concentration in the reported oxide materials.[54–56] The EPR spectra of the SMAO:Eu^{2+} samples are shown in Fig. 5e, and the signal g = 1.98 can be assigned to V_O.[57] By comparing the EPR signals of the SMAO host with that of the SMAO:0.015Eu^{2+} sample, it can be found that more V_O are formed in the SMAO:0.015Eu^{2+} sample when both types of samples are sintered in a reducing atmosphere simultaneously. Therefore, sufficient evidence proves that the defects of zero-thermal-quenching behavior are ascribed to V_O in the sample. The zero-thermal-quenching behavior can be further illustrated by the mechanism diagram in Fig. 5f. The ground state electrons are excited to the 5d orbital under external excitation, and some electrons are captured by traps under the conduction band and then escape from the traps as the temperature increases. In this process, the number of emitted photons exceeds the number of photons attenuated due to thermal quenching; hence, the overall emission intensity exhibits an increasing trend. The aforementioned studies indicate that the excellent thermal stability of the SMAO:0.015Eu^{2+} phosphor can be attributed to the continuous thermal defects within the system.

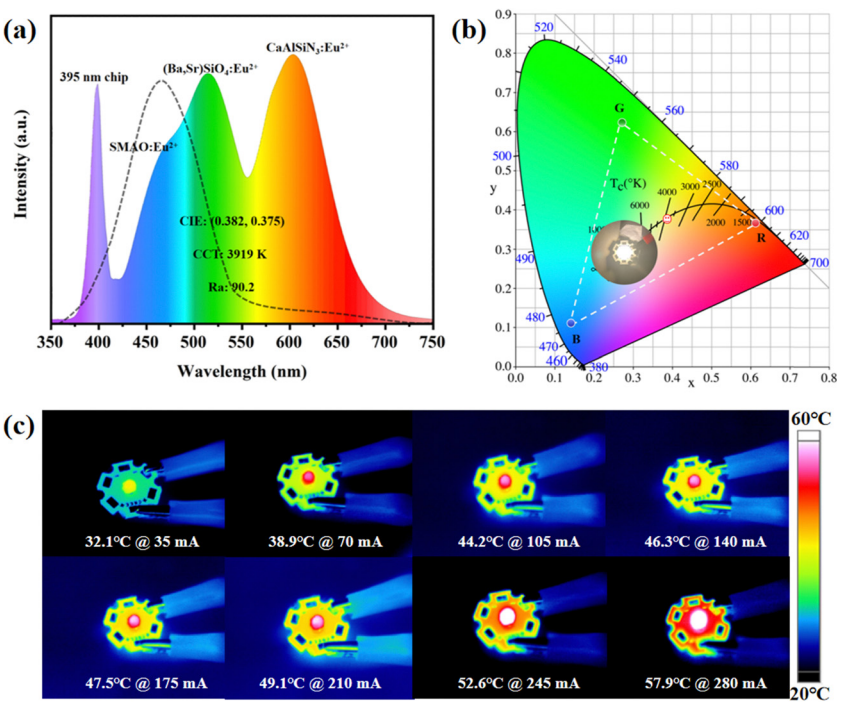

Fig. 6 (a) The electroluminescence spectrum of the WLED fabricated using a 395 nm chip. The melatonin suppression curve (dashed); (b) the photograph and CIE coordinates of LED lamp pack; (c) thermal images of the WLED device under various drive currents.

2.4 Human-centric WLED fabrication and electroluminescent property investigation

In order to reveal the potential application of the SMAO:Eu^{2+} phosphor in human-centric lighting, a prototype device was fabricated using a violet ($\lambda_{ex} \approx 395$ nm) LED chip and a blend of the SMAO:Eu^{2+} blue phosphor, commercial $(Ba,Sr)_2SiO_4$:Eu^{2+} green phosphor, and commercial $CaAlSiN_3$:Eu^{2+} red phosphor (Fig. 6a), with the corresponding luminescence photograph shown in Fig. 6b. The prototype ''LED'' device emits a bright warm white light and the corresponding CIE coordinates of WLED are (0.382, 0.375); the correlated color temperature (CCT) is 3919 K with an Ra value of 90.2. Finally, the production of human-centric warm WLEDs is analyzed through the wavelength-dependent melatonin suppression curve (dashed line). The blue light intensity produced by the device is significantly lower than the blue light intensity of the blue LED chips in commercial WLEDs.[8,9] This means that warm WLEDs packaged with the 395 nm chip and SMAO:Eu^{2+} blue phosphor can effectively reduce the blue light component without significantly interfering with the melatonin production. In addition, the thermal images of the WLED device under different driving currents taken using a thermal imaging camera are shown in Fig. 6c. The operating temperature is 57.9 °C at 280 mA, which indicates that SMAO:Eu^{2+} is promising for use in high power WLEDs. These results indicate that prototype devices based on the SMAO:Eu^{2+} phosphor as blue emitters have good prospects for sustainable and human-centric healthy lighting, while maintaining a high color rendering index and warm white light.

3. Conclusions

We have obtained a blue-emitting SMAO:Eu^{2+} phosphor that can be excited by LWUV light ($\lambda_{ex} \approx 395$ nm), which contains more cyan light and fewer blue light components compared with commercial BAM:Eu^{2+}. The optimal doping concentration of Eu^{2+} has been determined to be 0.015. The IQE of the SMAO:0.015Eu^{2+} phosphor under 395 nm excitation has been determined to be 70.76%, which is better than those of most of the blue luminescent materials that have been reported. More importantly, the IQE value of SMAO decreased by only 5% after prolonged exposure to air for 2.5 years, which is consistent with the concept of sustainable development. The SMAO:0.015Eu^{2+} phosphor exhibits better thermal stability than commercial BAM:Eu^{2+}, and the zero-thermal-quenching behavior of the SMAO:0.015Eu^{2+} phosphor can be attributed to the distribution of continuous traps generated by V_O in the SMAO:0.015Eu^{2+} sample. More satisfactorily, the incorporation of the SMAO:Eu^{2+} phosphor as a blue emitter in 395 nm LED chip pumping prototype devices can significantly reduce the intensity of blue light without noticeably affecting the melatonin production. This paper presents an excellent SMAO:Eu^{2+} blue phosphor, which not only promotes sustainable and human-centric lighting but also effectively will promote the future development of WLED lighting.

Data availability

The data that support the findings of this study are available in the ESI† of this article.

Author contributions

H. D. prepared the phosphorene samples and performed thermal treatment and photoluminescence characterization studies. H. D., Z. L., and X. W. analyzed the experimental data. J. Z. and G. Z. performed the theoretical calculations. H. D., G. Z., X. X. drafted the manuscript. All authors discussed and commented on the manuscript.

Conflicts of interest

The authors declare no conflict of interest.

Acknowledgements

This work was financially supported by the Yunnan Major Scientific and Technological Projects (No. 202202AG050004 and 202202AG050016), the International Joint Innovation Platform of Yunnan Province (No. 202203AP140004), the Science and Technology Talents and Platform Program (Workstation for Academicians and Experts) (No. 202205AF150005), the Yunnan Provincial Natural Science Foundation (No. 202101 AT070126), the National Natural Science Fund (No. 62375038 and 12174046), the LiaoNing Revitalization Talents Program (No. XLYC2007048), and the Dalian Science and Technology Innovation Fund (No. 2022JJ12GX041).

References

1 R. Nagare, M. Rea, B. Plitnick and M. Figueiro, Effect of white light devoid of ''cyan'' spectrum radiation on nighttime melatonin suppression over a 1-h exposure duration, *J. Biol. Rhythms.*, 2019, **34**, 195–204.
2 Y. Saw, V. Kalavally and C. Tan, The spectral optimization of a commercializable multi-channel led panel with circadian impact, *IEEE Access*, 2020, **8**, 136498–136511.
3 Y. Kim, P. Arunkumar, S. Park, H. Yoon and W. Im, Tuning the diurnal natural daylight with phosphor converted white led-advent of new phosphor blend composition, *Mater. Sci. Eng. B*, 2015, **193**, 4–12.
4 M. Zhao, Q. Y. Zhang and Z. G. Xia, Narrow-band emitters in LED backlights for liquid-crystal displays, *Mater. Today*, 2020, **40**, 246–265.
5 J. Oh, S. Yang and Y. Do, Healthy, natural, efficient and tunable lighting: four-package white leds for optimizing the circadian effect, color quality and vision performance, *Light: Sci. Appl.*, 2014, **3**, e141.
6 J. Gao, Z. G. Xia, Q. Ding, Y. P. Liu, P. Yan, Y. F. Hu, L. J. Wang, W. Luo, Y. C. Fan and W. Jiang, Cold sintering of highly transparent calcium fluoride nanoceramic as a

universal platform for high-power lighting, *Adv. Funct. Mater.*, 2023, **33**, 2302088.
7 K. Houser, P. Boyce, J. Zeitzer and M. Herf, Human-centric lighting: myth, magic or metaphor, *Lighting Res. Technol.*, 2021, **53**, 97–118.
8 Y. L. Xue, Y. J. Liang, W. L. Zhang, Y. Dou, Q. K. Wang, X. D. Wu and Y. S. Han, High performance of broad excitation and narrow emission green phosphor $NaAl_{11}O_{17}:Eu^{2+}$, Mn^{2+} for backlight displays, *J. Mater. Chem. C*, 2023, **11**, 10535–10546.
9 S. Pimputkar, J. Speck, S. DenBaars and S. Nakamura, Prospects for LED lighting, *Nat. Photonics*, 2009, **3**, 180–182.
10 S. Allen and A. Steckl, A nearly ideal phosphor-converted white light-emitting diode, *Appl. Phys. Lett.*, 2008, **92**, 143309.
11 H. X. Liao, M. Zhao, Y. Y. Zhou, M. S. Molokeev, Q. L. Liu, Q. Y. Zhang and Z. G. Xia, Polyhedron transformation toward stable narrow-band green phosphors for wide-color-gamut liquid crystal display, *Adv. Funct. Mater.*, 2019, **29**, 1901988.
12 J. Liebmann, M. Born and V. Kolb-Bachofen, Blue-light irradiation regulates proliferation and differentiation in human skin cells, *J. Invest. Dermatol.*, 2010, **130**, 259–269.
13 L. Mure, F. Vinberg, A. Hanneken and S. Panda, Functional diversity of human intrinsically photosensitive retinal ganglion cells, *Science*, 2019, **366**, 1251–1255.
14 A. Prayag, M. Munch and C. Gronfier, Light modulation of human clocks, wake, and sleep, *Clocks Sleep*, 2019, **1**, 193–208.
15 Q. Zhang, X. Ding, H. Y. Wang, B. Liu and Y. H. Wang, A novel narrow-band blue-emitting phosphor with high efficiency and thermal stability for WLEDs and FEDs, *J. Mater. Chem. C*, 2023, **11**, 15366–15395.
16 ICNIRP, Light-emitting diodes (LEDS): implications for safety, *Health Phys.*, 2020, **118**, 549–561.
17 L. Wu, S. J. Sun, Y. X. Bai, Z. G. Xia, L. W. Wu, H. M. Chen, L. R. Zheng, H. Yi, T. Q. Sun, Y. F. Kong, Y. Zhang and J. J. Xu, Defect-induced self-reduction and anti-thermal quenching in $NaZn(PO_3)_3:Mn^{2+}$ red phosphor, *Adv. Opt. Mater.*, 2021, **9**, 2100870.
18 D. W. Wen, H. M. Liu, Z. Ma, L. Zhou, J. H. Li, Y. Guo, Q. G. Zeng, P. A. Tanner and M. M. Wu, Improved thermal and chemical stability of oxynitride phosphor from facile chemical synthesis for vehicle cornering lights, *Angew. Chem. Int. Ed.*, 2023, **62**, e202307868.
19 M. Zhao, Y. Y. Zhou, M. S. Molokeev, Q. Y. Zhang, Q. L. Liu and Z. G. Xia, Discovery of new narrow-band phosphors with the UCr_4C_4-related type structure by alkali cation effect, *Adv. Opt. Mater.*, 2019, **7**, 1801631.
20 S. Piao, Y. Wang, X. Li and B. Chen, Defect engineering in a Eu^{2+}-doped β-Al_2O_3 structure blue phosphor and its controllable zero-thermal-quenching luminescence, *ACS Sustainable Chem. Eng.*, 2021, **9**, 7882–7890.
21 Y. Shao, H. Cai, Z. Song and Q. Liu, Efficient violet-light-excitable blue-cyan phosphor for full-spectrum lighting, *Inorg. Chem. Front.*, 2022, **9**, 5590–5596.
22 C. Lee, C. Wu, H. Li and C. Yang, Synthesis and luminescence properties of Eu^{2+}-doped $Sr_3MgSi_2O_8$ blue light-emitting phosphor for application in near-ultraviolet excitable white light-emitting diodes, *Nanomaterials*, 2022, **12**, 2706.
23 J. Zheng, S. Wu, Q. Cheng and C. Chen, Blue-emitting $Ca_5(PO_4)_3Cl:Eu^{2+}$ phosphor for near-UV pumped light emitting diodes: electronic structures, luminescence properties and LED fabrications, *J. Alloys Compd.*, 2016, **663**, 332–339.
24 S. Oshio, T. Matsuoka, S. Tanaka and H. Kobayashi, Mechanism of luminance decrease in $BaMgAl_{10}O_{17}:Eu^{2+}$ phosphor by oxidation, *J. Electrochem. Soc.*, 1998, **145**, 3903–3907.
25 K. Mishra, M. Raukas, G. Marking, P. Chen and P. Boolchand, Investigation of fluorescence degradation mechanism of hydrated $BaMgAl_{10}O_17$:Eu2+ phosphor, *J. Electrochem. Soc.*, 2005, **152**, H183–H190.
26 S. Hariyani and J. Brgoch, Advancing human-centric LED lighting using $Na_2MgPO_4F:Eu^{2+}$, *ACS Appl. Mater. Interfaces*, 2021, **13**, 16669–16676.
27 Z. Leng, H. Bai, Z. Tang, F. Song and H. Wu, A zero-thermal-quenching blue phosphor for sustainable and human-centric WLED lighting, *ACS Sustainable Chem. Eng.*, 2022, **10**, 10966–10977.
28 Q. Wang, H. Dong and F. Wu, Ratiometric optical thermometer with high sensitivity based on dual far-red emission of Cr^{3+} in $Sr_2MgAl_{22}O_{36}$, *Ceram. Int.*, 2019, **46**, 5008–5014.
29 Z. Li, G. Zhu, X. Luo, M. He and B. Dong, Ultra-small stokes shift induced thermal robust efficient blue-emitting alkaline phosphate phosphors for LWUV WLEDs, *Ceram. Int.*, 2023, **49**, 21510–21520.
30 D. Zhang, X. Zhang, Y. Song and H. Zou, Li^+ ion induced full visible emission in single Eu^{2+}-doped white emitting phosphor: Eu^{2+} site preference analysis, luminescence properties, and WLED applications, *Adv. Optical Mater.*, 2021, **9**, 2100337.
31 D. Wu, J. Si, G. Xie, J. Huang and G. Cai, Two-site occupancy induced a broadband blue-emitting in Eu^{2+} doped $Na_3Ba_2Ca(PO_4)_3$ phosphor, *Ceram. Int.*, 2023, **49**, 34805–34813.
32 C. Xie, L. Mei, J. Chen, J. Yang and D. Liu, Simultaneous spectral tuning and thermal stability adjustment in $Ca_8ZnGa_{(1-x)}La_x(PO_4)_7:Eu^{2+}$ phosphors, *Inorg. Chem.*, 2022, **61**, 3263–3273.
33 Y. Fu, P. Xiong, Q. Liu, M. Peng and Y. Chen, A promising blue-emitting phosphor $CaYGaO4:Bi^{3+}$ for near ultraviolet (NUV) pumped white LED application and the emission improvement by Li^+ ions, *J. Mater. Chem. C*, 2021, **9**, 303–312.
34 Q. Wu, Y. Li, S. Ye, L. Zhao, J. Ding and J. Zhou, A novel narrow-band blue-emitting phosphor of Bi^{3+}-activated $Sr_3Lu_2Ge_3O_{12}$ based on a highly symmetrical crystal structure used for WLEDs and FEDs, *Chem. Eng. J.*, 2020, **401**, 126130.
35 K. Shioi, N. Hirosaki, R. Xie, T. Takeda and Y. Li, Luminescence properties of $SrSi_6N_8:Eu^{2+}$, *J. Mater. Sci.*, 2008, **43**, 5659–5661.

36 X. Wang, Z. Zhao, Y. Li and Y. Wang, Structure, photoluminescence and abnormal thermal quenching behavior of Eu^{2+}-doped $Na_3Sc_2(PO_4)_3$: a novel blue-emitting phosphor for n-UV LEDs, *J. Mater. Chem. C*, 2016, **4**, 8795–8801.

37 D. Wang, Y. Wu and T. Chen, Synthesis, crystal structure, and photoluminescence of a novel blue-green emitting phosphor: $BaHfSi_3O_9$:Eu^{2+}, *J. Mater. Chem.*, 2011, **21**, 18261–18265.

38 D. Gao, Q. Kuang, F. Gao, H. Xin, S. Yun and Y. Wang, Achieving opto-responsive multimode luminescence in $Zn_{1+x}Ga_{2-2x}Ge_xO_4$: Mn persistent phosphors for advanced anti-counterfeiting and information encryption, *Mater. Today Phys.*, 2022, **27**, 100765.

39 Z. Xia, R. Liu, K. Huang and V. Drozd, $Ca_2Al_3O_6F$:Eu^{2+}: a green-emitting oxyfluoride phosphor for white light-emitting diode, *J. Mater. Chem.*, 2012, **22**, 15183–15189.

40 L. Yan, G. Zhu, X. Luo and B. Dong, Emerging Fe^{3+} doped broad nir-emitting phosphor $Ca_{2.5}Hf_{2.5}(Ga, Al)_3O_{12}$:$Fe^{3+}$ for LWUV pumped NIR LED, *Laser Photonics Rev.*, 2024, **18**, 2301200.

41 D. Zhao, S. R. Zhang, R. J. Zhang, B. Z. Liu and Q. X. Yao, Warm white light emission, thermochromic property and long persistent luminescence derived from multi-sites of Eu^{2+}/Eu^{3+} in host lattice, *Chem. Eng. J.*, 2022, **428**, 131023.

42 D. Zhao, Y. L. Xue, R. J. Zhang, Y. P. Fan, B. Z. Liu, Y. N. Lia and S. R. Zhang, Design, synthesis, crystal structure and luminescent properties introduced by Eu^{3+} of a new type of rare-earth borophosphate $CsNa_2REE_2(BO_3)(PO_4)_2$ (REE = Y, Gd), *Dalton Trans.*, 2020, **49**, 10104–10113.

43 Y. Wei, L. Cao, H. Jang, P. Dang and J. Lin, Highly efficient blue emission and superior thermal stability of $BaAl_{12}O_{19}$:Eu^{2+} phosphors based on highly symmetric crystal structure, *Chem. Mater.*, 2018, **30**, 2389–2399.

44 P. Dai, Q. Wang, T. Chan and X. Wang, Composition-driven anionic disorder-order transformations triggered single-Eu^{2+}-converted high-color-rendering white-light phosphors, *Chem. Eng. J.*, 2020, **380**, 122508.

45 R. Song, Y. Zheng, K. Xiong and J. Zhu, Charge compensation and solid-state lighting application for dysprosium-activated $Ba_2TeP_2O_9$ phosphor, *J. Alloys Compd.*, 2022, **912**, 165188.

46 Y. Chen, Q. Guo, L. Liao, M. Runowski and B. Ma, Preparation, crystal structure and luminescence properties of a novel single-phase red emitting phosphor $CaSr_2(PO_4)_2$: Sm^{3+}, Li+, *RSC Adv.*, 2019, **9**, 4834–4842.

47 R. Shi, X. Zhang, Z. Qiu, X. Xu, L. Yu and S. Lian, Composition and antithermal quenching of noninteger stoichiometric Eu^{2+}-doped Na-β-alumina with cyan emission for near-UV WLEDs, *Inorg. Chem.*, 2021, **60**, 19393–19401.

48 D. Zhao, S. Zhang, Y. Fan, B. Liu and R. Zhang, Thermally stable phosphor $KBa_2(PO_3)_5$:Eu^{2+} with broad-band cyan emission caused by multisite occupancy of Eu^{2+}, *Inorg. Chem.*, 2020, **59**, 8789–8799.

49 Q. Zhang, X. Ding, H. Wang, B. Liu and Y. Wang, A novel narrow-band blue-emitting phosphor with high efficiency and thermal stability for WLEDs and FEDs, *J. Mater. Chem. C*, 2023, **11**, 15366–15375.

50 W. Li, Y. Zhuang, S. Tanabe and R. Xie, Tailoring trap depth and emission wavelength in $Y_3Al_{5-x}Ga_xO_{12}$:Ce^{3+}, V^{3+} phosphor-in-glass films for optical information storage, *ACS Appl. Mater. Interfaces*, 2018, **10**, 27150–27159.

51 R. Shi, L. Ning and H. Liang, Zero-thermal quenching of Mn^{2+} red luminescence via efficient energy transfer from Eu^{2+} in $BaMgP_2O_7$, *Adv. Optical Mater.*, 2019, **7**, 1901187.

52 V. Rajendran, T. Lesniewski, S. Mahlik, M. Grinberg and R. Liu, Ultra-broadband phosphors converted near-infrared light emitting diode with efficient radiant power for spectroscopy applications, *ACS Photonics*, 2019, **6**, 3215–3224.

53 Y. Wei, G. Xing and J. Lin, New strategy for designing orangish-red-emitting phosphor via oxygen-vacancy induced electronic localization, *Light: Sci. Appl.*, 2019, **8**, 1–9.

54 F. Kang, X. Yang, Q. Zhang and J. Qiu, Red photoluminescence from Bi^{3+} and the influence of the oxygen-vacancy perturbation in $ScVO_4$: a combined experimental and theoretical study, *J. Phys. Chem. C*, 2014, **118**, 7515–7522.

55 Y. Zhang, X. Shan, W. Wang and Y. Liang, Multimodal luminescence in Pr^{3+} single-doped Li_2CaSiO_4 phosphor for optical information storage and anti-counterfeiting applications, *Chem. Eng. J.*, 2023, **474**, 145886.

56 X. Han, C. Hu, J. Wu, S. Wang, Z. Ye and Q. Yang, Systematical site investigation and temperature sensing in Pr^{3+}-doped $M_3RE_4O_9$ (M = Sr and Ba; RE = Sc, Y, Lu), *Chem. Eng. J.*, 2023, **452**, 139159.

57 Z. Li, G. Zhu, S. Xin and B. Dong, High-performance NIR emission in chromium-doped garnet phosphors enabled by structure and excitation regulation, *Laser Photonics Rev.*, 2024, **18**, 2300732.